A 2D/3D FINITE VOLUME METHOD USED TO SOLVE THE BIDOMAIN EQUATIONS OF ELECTROCARDIOLOGY*

YVES COUDIÈRE†, CHARLES PIERRE‡, AND RODOLPHE TURPAULT†

Abstract. This paper presents the resolution of the direct problem of electrocardiology by a new 2D/3D finite volume technique. The most up-to-date model of electrocardiology is used: the bidomain equations together with realistic ionic models of the cell membrane inside the heart is fully coupled to the electrostatic behavior of the torso. Several numerical results are shown.

Key words. Finite volume methods, Bidomain equations, Electrocardiology.

AMS subject classifications. 35J65, 65N15, 74S10

1. Introduction. The bidomain model is the best for electrophysiology computations at the scale of the myocardial ventricle or the whole heart. Although it is by far the more complex and numerically expensive [KS98, CFDE⁺05] essentially because it requires, in any case, to solve a large and ill-conditioned linear system at each computational time-step. The bidomain model is a system of degenerate semilinear parabolic equations with a reaction term that is coupled at each point to a large set of stiff differential equations (ionic model), representing the physiological behavior of the cell membrane at a microscopic level. Its solutions are composed of sharp propagating wave fronts, that generate a non-stationary electrical field. The measures of this electrical field at the body surface are the well known electrocardiograms (ECG).

Hence, modeling the ECG requires to couple the bidomain equations to the evolution of the extracardiac electrical field. The coupling occurs through flux continuity conditions at the interface heart/torso.

In this paper, we propose a new approach to compute some ECGs using the bidomain equations together with a realistic ionic model, of Luo-Rudy type [FR00, SR97] and the coupling relations from [KN94]. In particular, the continuity of the current fluxes at the heart/torso interface is achieved exactly for the numerical solution, from a finite volume technique: finite volume techniques are based on flux approximation and flux conservativity properties. Other studies [CFDE⁺05, LBG⁺03] using finite element techniques only ensure the flux continuity relation in a weak sense, through a variational formulation of the problem.

The numerical method is a 2D and 3D *discrete duality finite volume* technique exposed in [CPT08, Pie05]. The discrete problem is proved to be well-posed. This paper furthermore presents several numerical experiments and investigates some practical aspects of ECG computations, like preconditioning of the linear system and profiling of the different parts of the computations.

Section 2 introduces the basics of ECG modeling and section 3 briefly summarizes the finite volume technique. The technique to solve the discrete problem is explained

---

†Laboratoire de Mathématiques Jean Leray, CNRS - Université de Nantes - ÉCN, UMR 6629 (`Yves.Coudiere@univ-nantes.fr`).

‡ Laboratoires de Mathématiques et de leurs Applications, CNRS - Université de Pau et des Pays de l'Adour, UMR 5142 (`Charles.Pierre@univ-pau.fr`).

in section 4. Section 5 and 6 are devoted to the exposition and comments of numerical experiments.

2. Principles of the computation of ECGs.

2.1. The bidomain equations. The computational domain Ω is split as described on figure 2.1: the heart H and torso T domains are open bounded polygonal subsets of $\mathbb{R}^d$ ($d = 2, 3$). The boundary of Ω is denoted by Γ and the heart-torso interface is denoted by $\Sigma = \bar{H} \cap \bar{T}$. The unit normal to Σ pointing from H towards T is $\mathbf{n}_\Sigma$, and Γ is split into Γ^1 and Γ^2.
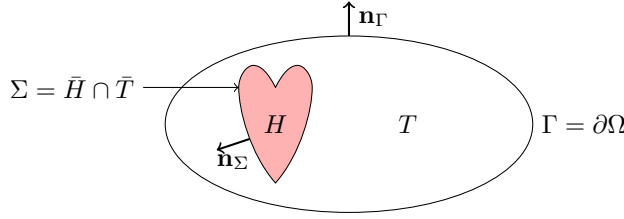

FIGURE 2.1. *Heart H and Torso T, the computational domain is $\Omega = H \cup \Sigma \cup T$.*

The bidomain model represents the heart tissue at a macroscopic scale as the superimposition of some intra- and extracellular media. It is a homogeneization point of view. An intra- and an extracellular electrical potential, namely u_i and u_e, are defined on the whole heart domain H. Their difference is called *the transmembrane potential* and denoted by $u = u_i - u_e$. At a microscopic level, the transmembrane potential is set only on the cell membrane, that has a capacitive behavior. At a macroscopic level, the current balance reads in H:

$$A_m \left(C_m \partial_t u + I_{ion}(t; u, \ldots) - I_{stim}(t, x) \right) = -\operatorname{div}(G_e \nabla u_e), \qquad (2.1)$$

where A_m is the cell membrane surface to volume ratio, C_m is the membrane capacitance per unit area, I_{ion} is the current induced by some biochemical ionic processes described below, I_{stim} is a given current of stimulation and G_e is the conductivity of the extracellular medium.

Using $u_i = u + u_e$, the quasistatic electrical equilibrium for u_T, u_e, u_i reads

$$\operatorname{div}\left((G_i + G_e)\nabla u_e \right) = -\operatorname{div}\left(G_i \nabla u \right) \quad \text{in } H, \quad \text{and } \operatorname{div}\left(G_T \nabla u_T \right) = 0 \quad \text{in } T, \quad (2.2)$$

while it is assumed the following relationships for the flux of current:

$$G_i \nabla u_e \cdot \mathbf{n}_\Sigma = -G_i \nabla u \cdot \mathbf{n}_\Sigma, \quad G_e \nabla u_e \cdot \mathbf{n}_\Sigma = -G_T \nabla u_T \cdot \mathbf{n}_\Sigma \text{ (on } \Sigma), \qquad (2.3)$$

$$G_T \nabla u_T \cdot \mathbf{n}_\Omega = 0 \text{ (on } \Gamma^2), \quad u_T = 0 \text{ (on } \Gamma^1). \qquad (2.4)$$

The main unknowns are the three functions u, u_e, u_T respectively defined on $[0, +\infty) \times H$, $[0, +\infty) \times H$ and $[0, +\infty) \times T$. The conductivities G_i, G_e, G_T are supposed to be matrix valued smooth functions respectively on $\bar{H}$, $\bar{H}$ and $\bar{T}$, and to be *uniformly elliptic*. The first condition in eq (2.3) means that no current flows out of the heart from the intracellular medium ($u_i = u + u_e$), as it as been shown by physiological data at the cellular scale. The remaining conditions express that the interaction between the heart and the torso is achieved via the extracellular domain.

At last, a solution to the bidomain equation is a solution to the evolution equations (2.1) coupled to the elliptic equations (2.2) through the interface conditions (2.3)

and with the boundary condition (2.4). The global system has a variational formulation and the evolution equation (2.1) cannot be decoupled from the quasistatic balance equations (2.2) because of the coupling condition.

2.2. Ionic current. The ionic current I_{ion} which appears in eq. (2.1) represents the current generated by the movement of ions through the cell membrane. It is due to several processes. For instance, an *ionic channel p* (a protein) specific to ion X is responsible for an ionic current given by Ohm's law, $i_{X,p} = g_{X,p}(u - E_X)$, where E_X is the equilibrium potential given by Nernst's law, $E_X = \frac{RT}{F} ln \left(\frac{[X]_e}{[X]_i} \right)$, and $g_{X,p}$ is the conductivity. Channels may involve complex behavior and only allow a given ion to pass under particular conditions. The conductivity may therefore be written: $g_{X,p} = \bar{g}_{X,p} f(u, [X], \dots)$, where $\bar{g}_{X,p}$ is the maximum conductivity and f a function that ranges from 0 (closed) to 1 (open). As an example, the fast-Na^+ current is

$$i_{Na} = g_{Na}(u - E_{Na}). \tag{2.5}$$

The conductivity can be expressed with an Hodgkin-Huxley formalism as $g_{Na} = \bar{g}_{Na} m^3 h j$ where m, h and j are activation or inactivation gates ruled by ordinary differential equations (ODE) e.g.:

$$d_t h = \alpha_h (1 - h) - \beta_h h \tag{2.6}$$

where α_h and β_h are physiological parameters which may depend on various variables (u, concentrations, $t,\dots$). As a result the value of I_{ion}, which is the sum of all ionic currents through the membrane, depends on the resolution of several non-trivial ODE. Depending on the model, the number of these equations varies from three to a few dozen.

Complex models also involve pumps, exchangers and buffers in order to have a more realistic behavior, for example in the determination of the intracellular calcium concentration which is directly responsible of the muscular contraction.

At last, the ionic current appears as a function

$$I_{ion} = I_{ion}(t, u, [X]_i, [X]_e, \mathbf{w}), \tag{2.7}$$

where $[X]_{i,e}$ are the intra- and extracellular concentrations of ions X (Na, K, Ca) and $\mathbf{w}$ is a vector collecting the gate variables.

For more information it is recommended to refer to the huge literature on the subject. Specifically, the numerical experiments in this paper make use of the models specified in [SR97, FR00].

2.3. Initial data. Initial data are provided for the concentration $[X]_{i,e}$, the gate variables $\mathbf{w}$ and the transmembrane potential u only, since u_e is defined by equation (2.2), as proved in [BCP09].

3. The finite Volume Approach. The bidomain system of equation consists in eqs. (2.1)-(2.2) with interface and boundary conditions (2.3) and (2.4), where I_{ion} is computing according to eq. (2.7) after solving a system of the form of eqs. (2.5) and (2.6). It involves two anisotropic diffusion operators with distinct and space-dependant coefficients; an isotropic one (in the torso); and a transmission (discontinuous coefficient) condition. The meshes, eventually derived from medical images, might be distorded. The Discrete Duality Finite Volume method is well suited for this problem. It is robust, accurate and it handles naturally the transmission conditions

(2.3) because they are conditions on the flux. For 2D computations, the method has been adapted from [DO05] to take into account discontinuous coefficients. For 3D computation an innovative construction of the DDFV scheme is used. It has been explained in [CPT08, Pie05].

3.1. The principle of the DDFV method. Suppose that $\mathcal{M} = \{K, \text{convex polygon}\}$ is a finite volume mesh[1] of Ω. The symbols $\mathcal{S}$ and $\mathcal{V}$ refer respectively to the sets of interfaces σ and vertexes a of the mesh $\mathcal{M}$. The mesh is assumed to be such that $\Sigma = \cup_{\sigma \in \mathcal{S}_\Sigma} \sigma$ for a subset $\mathcal{S}_\Sigma$ of $\mathcal{S}$, in such a way that $\mathcal{M}$ can be split into two complementary parts, $\mathcal{M}_H$ and $\mathcal{M}_T$ that are finite volume meshes of H and T respectively. Hence the interfaces and vertexes of $\mathcal{M}_H$ and $\mathcal{M}_T$ are respectively denoted by $\mathcal{S}_H$, $\mathcal{S}_T$ and $\mathcal{V}_H$, $\mathcal{V}_T$. Note that $\mathcal{S}_H \cap \mathcal{S}_T = \mathcal{S}_\Sigma$. Similarly, the set of the vertexes of $\mathcal{M}$ that belongs to Σ is denoted by $\mathcal{V}_\Sigma$ and verifies $\mathcal{V}_\Sigma = \mathcal{V}_H \cap \mathcal{V}_T$.

The finite volume unknown for the bidomain system of equations is a set of scalar values $u_\mathcal{M} = \{(u_K)_{K \in \mathcal{M}_H}, (u_a)_{a \in \mathcal{V}_H}\}$ that approximates u and a set $v_\mathcal{M} = \{(v_K)_{K \in \mathcal{M}}, (v_a)_{a \in \mathcal{V}}\}$ that approximate the function $v(x) = u_e(x)$ if $x \in H$ and $u_T(x)$ if $x \in T$. This is possible because $u_e(x) = u_T(x)$ along Σ (eq. (2.2) with (2.3) is a transmission problem). Of course there are also unknowns defined on the $K \in \mathcal{M}_H$ and $a \in \mathcal{V}_H$ for the ionic current I_{ion} and the state variables of the ionic models, $[X]_e$, $[X]_i$ and $\mathbf{w}$.

Around each vertex $a \in \mathcal{V}$ is built a control volume denoted by A, by joining the centers of gravity and the midpoints of the cells and edges that share a as a common vertex. The idea of the method is to write two finite volumes schemes on the two families of control volumes ($K \in \mathcal{M}$ and A for $a \in \mathcal{V}$). These schemes involve the computation of approximate fluxes on the interfaces between the control volumes. These fluxes rely on a consistent approximation of the gradients of $u_\mathcal{M}$ and $v_\mathcal{M}$.

With unknown values located at each vertex a and each cell K of $\mathcal{M}$, it is easy to built a consistent approximation of the gradient of $u_\mathcal{M}$ and $v_\mathcal{M}$. It is defined piecewise on some *diamond* cells, defined as $D_{\sigma,K} = \text{hull}(\sigma, x_K)$ for any $K \in \mathcal{M}$ and any interface $\sigma \subset \partial K$. To treat the discontinuity of the conductivity matrix along Σ, an auxiliary unknown is defined on σ that is algebraically eliminated using the consistency relationship (see [CPT08])

$$G_K \nabla_{\sigma,K} u_\mathcal{M} \cdot \mathbf{n}_{\sigma,K} = G_L \nabla_{\sigma,L} u_\mathcal{M} \cdot \mathbf{n}_{\sigma,L} \quad (\sigma = K \cap L, \ K, L \in \mathcal{M}). \qquad (3.1)$$

In this relation, G may stand for G_e, $G_i + G_e$, G_i or G_T depending on the equation considered. If $G_K = G_L$, the formula for the gradient is the usual diamond scheme one, otherwise, it involves an harmonic mean of G_K and G_L [Pie05].

The conductivity matrices are approximated by their mean values inside each control volume K or A, $G_K = \frac{1}{|K|} \int_K G(x)dx$ and $G_a = \frac{1}{|A|} \int_A G(x)dx$ ($|K|$ and $|A|$ denote the 3D lebesgue measure of the sets K and A).

3.2. The discrete bidomain system of equations. As a consequence, the semi-discrete system of equations on $u_\mathcal{M}$ reads, for all $K \in \mathcal{M}_H$ and $a \in \mathcal{V}_H$,

$$A_m(C_m d_t u_K + I_{ion,K} - I_{stim,K})|K| = - \sum_{\sigma \in \delta K} G_{e,K} \nabla_{\sigma,K} v_\mathcal{M} \cdot N_{\sigma,K} \qquad (3.2)$$

$$A_m(C_m d_t u_a + I_{ion,a} - I_{stim,a})|A| = - \sum_{(\sigma,K) \in \delta a} G_{e,K} \nabla_{\sigma,K} v_\mathcal{M} \cdot N_{\sigma,K,a}, \qquad (3.3)$$

---

[1] that is a partition of Ω into non-overlapping control volumes

where δK is the subset of $\mathcal{S}$ such that $\partial K = \cup_{\delta K} \sigma$, $N_{\sigma,K}$ denotes the normal to σ outward of K with length equal to $|\sigma|$, δa denotes the subset of $\mathcal{S} \times \mathcal{M}$ associated to the boundary of A and $N_{\sigma,K,a}$ is the corresponding normal.

This evolution equation is coupled to the quasistatic balance equation on $v_{\mathcal{M}}$:

$$\forall K \in \mathcal{M}, \quad -\sum_{\sigma \in \delta K} G_K \nabla_{\sigma,K} v_{\mathcal{M}} \cdot N_{\sigma,K} = F_K, \tag{3.4}$$

$$\forall a \in \mathcal{V}, \quad -\sum_{(\sigma,K) \in \delta a} G_K \nabla_{\sigma,K} v_{\mathcal{M}} \cdot N_{\sigma,K,a} = F_a, \tag{3.5}$$

where the conductivity matrix is defined inside each $K \in \mathcal{M}$ by

$$G_K = \begin{cases} G_{i,K} + G_{e,K} & \text{if } K \in \mathcal{M}_H, \\ G_{T,K} & \text{if } K \in \mathcal{M}_T, \end{cases}$$

and the right-hand side is given by

$$F_K = \begin{cases} \sum_{\sigma \in \delta K} G_{i,K} \nabla_{\sigma,K} u_{\mathcal{M}} \cdot N_{\sigma,K} & \text{if } K \in \mathcal{M}_H, \\ 0 & \text{if } K \in \mathcal{M}_T, \end{cases}$$

$$F_a = \sum_{(\sigma,K) \in \delta a} \left(G_{i,K} \nabla_{\sigma,K} u_{\mathcal{M}} \cdot N_{\sigma,K} \right) \mathbf{1}_{K \in \mathcal{M}_H}$$

where $\mathbf{1}_{K \in \mathcal{M}_H} = 1$ if $K \in \mathcal{M}_H$ and 0 otherwise. The last definition covers the three distinct situations: $a \in \mathcal{V}_H \backslash \mathcal{V}_\Sigma$ for which $(\sigma, K) \in \delta a \Rightarrow K \in \mathcal{M}_H$, $a \in \mathcal{V}_T \backslash \mathcal{V}_\Sigma$ for which $(\sigma, K) \in \delta a \Rightarrow K \in \mathcal{M}_V$ and then $F_a = 0$ and the mixed situation $a \in \mathcal{V}_\Sigma$.

An explicit time-stepping strategy is used to solve equations (3.2) to (3.5) with a time step $\Delta t > 0$, so that the discrete system reads

$$A_m \left(C_m \frac{u_{\mathcal{M}}^{n+1} - u_{\mathcal{M}}^n}{\Delta t} + I_{ion}^n - I_{stim}^n \right) = -B_e v_{\mathcal{M}}^n \quad (n \geq 0), \tag{3.6}$$

$$B v_{\mathcal{M}}^n = -B_i u_{\mathcal{M}}^n \quad (n \geq 0), \tag{3.7}$$

for the unknowns $(u_{\mathcal{M}}^n)_{n \in \mathbb{N}}$ with $u_{\mathcal{M}}^n \in \mathbb{R}^{n_{\mathcal{M}_H} + n_{\mathcal{V}_H}}$ and $(v_{\mathcal{M}}^n)_{n \in \mathbb{N}}$ with $v_{\mathcal{M}}^n \in \mathbb{R}^{n_{\mathcal{M}} + n_{\mathcal{V}}}$ and where B_e, B and B_i are DDFV matrices and $n_{\mathcal{M}_H}, n_{\mathcal{M}}, n_{\mathcal{V}_H}$ and $n_{\mathcal{V}}$ are respectively the number of control volumes in $\mathcal{M}_H$ and $\mathcal{M}$, and the number of vertexes in $\mathcal{V}_H$ and $\mathcal{V}$.

3.3. Main property of the scheme. The DDFV discrete gradient and divergence operators briefly described above are known to verify a duality property similar to the Green formula [DO05, ABH07, CPT08] that reads here (due to our homogeneous boundary conditions)

$$\left(\text{div}_{\mathcal{M}} G_{\mathcal{M}} \nabla_{\mathcal{M}} v_{\mathcal{M}}^1, v_{\mathcal{M}}^2 \right) + \left(G_{\mathcal{M}} \nabla_{\mathcal{M}} v_{\mathcal{M}}^1, \nabla_{\mathcal{M}} v_{\mathcal{M}}^2 \right) = 0$$

for any discrete functions $v_{\mathcal{M}}^1$ and $v_{\mathcal{M}}^2$. Using the vectorial notations of system (3.6)-(3.7), the inner product between two discrete functions $u_{\mathcal{M}}^1$ and $u_{\mathcal{M}}^2$ reads $(u_{\mathcal{M}}^1, u_{\mathcal{M}}^2) = (u_{\mathcal{M}}^1)^T M u_{\mathcal{M}}^2$ where M is a diagonal mass matrix, $M_{KK} = |K|$ and $M_{aa} = |A|$. As a consequence, the matrices MB, MB_i, MB_e are symmetric and non negative and the linear system (3.7) has a unique solution. The semi-discrete problem is well-posed.

4. Resolution of the bidomain equations. At time $t^n = n\Delta t$ ($n \geq 0$), we successively

1. solve the linear system (3.7) in order to find $v_{\mathcal{M}}^n$;
2. compute the ionic current $I_{ion}^n = I_{ion}^n(t^n, u_{\mathcal{M}}^n, [X]_{i,\mathcal{M}}^n, [X]_{e,\mathcal{M}}^n, \mathbf{w}_{\mathcal{M}}^n)$ and update the state variables of the ionic model ,$[X]_{i,\mathcal{M}}^{n+1}, [X]_{e,\mathcal{M}}^{n+1}, \mathbf{w}_{\mathcal{M}}^{n+1}$;
3. finally update the transmembrane potential: compute $u_{\mathcal{M}}^{n+1}$ from (3.6)

The last point is straightforward, once the first two ones are correctly achieved.

4.1. The linear system. Its size is $n_{\mathcal{M}} + n_{\mathcal{V}}$ (the number of control volumes and vertexes – except the Dirichlet ones) and it must be solved for each time step. The numerical method to handle it has to be wisely chosen. Two methods seem particularly appropriate:

1. A bi-conjugate gradient algorithm, due to lack of symmetry in (3.7). In that case, the BICGStab improvement is used.
2. A GMRes algorithm is also possible after symmetrizing (3.7) with the diagonal mass matrix M. This symmetrization does only depend on the measures of our volumes and can simply be viewed as a preconditioner.

Moreover the anisotropies, mesh structures as well as the size of the problem cause the system to be very ill-conditioned most of the times. Hence a good choice of preconditioner can drastically improve the convergence. First of all, to cope with the distorted profile of the sparse matrix B, due to unstructured meshes, the unknowns are renumbered with the symmetric reverse Cuthill-McKee (SRCM) algorithm. Hence, a simple incomplete LU algorithm makes a very good preconditioner. Therefore, our choice of preconditioning is to stack the SRCM and ILU(p) matrices -and the symmetrizer before GMRes. Most of the times setting p to 0 or 1 is the most efficient choice since higher p require much more operations and seldom reduce enough the number of iterations to be competitive (table 5.1). The preconditioner has only to be built once for all. Thus the resulting method proves to be quite efficient in our purpose.

4.2. The ionic model. The computation of ionic currents involves the treatment of gate variables and other processes (pumps, exchangers, buffers,...) most of them strongly dependent on at least one other variable (such as u). While it is obviously crucial to perform a relevant approximation, it is also essential to avoid excessive computational costs. The methods used to make this approximation depends on the variables.

The greatest care was taken to compute the gates involved in the fast Na^+ current both because of its critical importance for the depolarization process and because of its very fast dynamics. In fact, during this depolarization, *a fourth-order Runge-Kutta method* is used if the time step overcome a threshold value. Aside from that case, these gates are treated as the others since their impact is then clearly less important.

Most of the gates and concentrations were updated using either an *Euler method* or an *analytical formula* assuming that u is constant inside each time step. This assumption proves to be particularly appropriate in the repolarization zones where u varies very slowly.

Finally, intracellular Ca^{2+} buffering is computed following the analytical formulation of Zeng et al [ZLRR95] which assume a steady-state for the buffering reaction.

These computations are purely local and very easy to parallelize. Moreover, profiled simulations have shown (see below) that only a very small amount of CPU time is required to compute the ionic current compared to the resolution of the linear system: choosing a more realistic model is not penalizing in terms of CPU time.

5. Numerical Experiments in a 2D model. In order to facilitate the comparisons, each of the following examples share the same geometry which mesh is shown in figure 5.1. A 8×6 cm elliptic heart with a ventricular cavity is placed inside a 15×8 cm torso. The mass potential is set near the middle of the northwest part of the border. The parameters were fixed to $A_m = 2000$ cm^{-1}, $C_m = 1$ μF.cm^{-2} and the intracellular and extracellular conductivities were respectively set to 4 mS.cm^{-1} and 2 mS.cm^{-1} in the fibers' direction and to 1.8 mS.cm^{-1} and 1.5 mS.cm^{-1} otherwise. The conductivity is also set to 2.39 mS.cm^{-1} inside the torso and Faber-Rudy's improvement [FR00] of Luo-Rudy II model is used for the computation of ionic currents. Finally all computations were carried out with the same time-step and for the same duration of 3 s, so that several successive heart-beats can be observed. There are 25570 DDFV unknowns for each of the variables.

FIGURE 5.1. *2D mesh with 8554 vertexes and 17016 triangles.*

5.1. Regular ECG. Two simulations have been carried out in the same conditions: with a stimulation that occurs every 600 ms for the Faber-Rudy model, that is at a rate of 100 bpm. The only difference is that the stimulus is placed on one site, on the axis at the left boundary between the heart and the ventricular cavity, in the first computation; and it is placed on two sites, on the left and the right of the ventricular cavity, in the second computation.

These two computations leads to the results shown on figure 5.2 and 5.3 on the top and bottom lines, respectively for the 1 site and 2 sites stimuli . The ECGs on figure 5.2 are extracted from 4 different points throughout the surface of the torso. The location of these electrodes is of course very important for the overall shape of the waves. The results show the huge impact of the presence of the second source term, as expected. Anyway, both QRS and T waves are easy to see and a regular beat can be observed.

The potential fields (figure 5.3) show the mechanisms of the evolution of $v = (u_e, u_T)$: since u_T does only depend on the values of u and u_e on the heart-torso interface Σ, it stays at rest until the wave reaches this interface; and then (figure 5.3) the whole torso is lit.

Profiling. On this simulation, the CPU time required by each part of the code has been profiled: for each time step, an average of 3.56% of the CPU time is spent for evaluating I_{ion} with Faber-Rudy's model [FR00] whereas 93.24% is spent for solving the linear system. Thus, even with a sophisticated ionic model, the time required for the computation of ionic process is not significant, which justifies the choice of realistic models compared to simplified ones.

5.2. Examples of irregular ECG. One of the edges of realistic models is the possibility to simulate various malfunctions. As an illustration, the results of *tachycardia* and *ischemia* are provided below.

Tachycardia results in an increase of the beat rate of the heart. Here, the stimulus is set to occur once every 250 ms (240 bpm) and the two-stimulus configuration
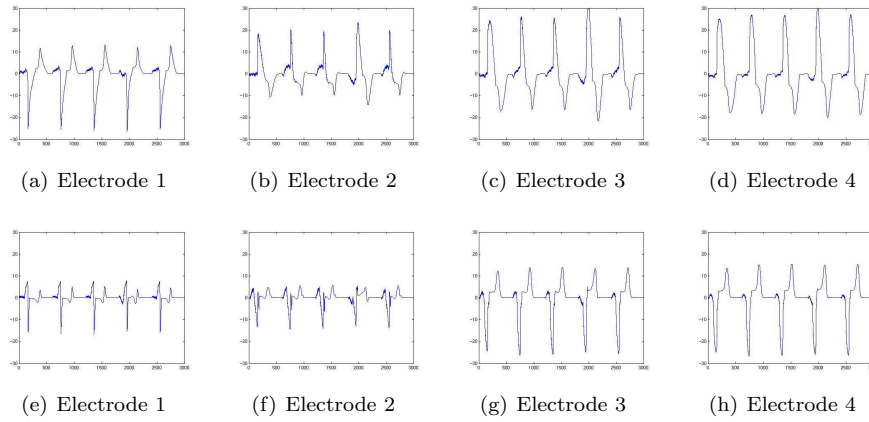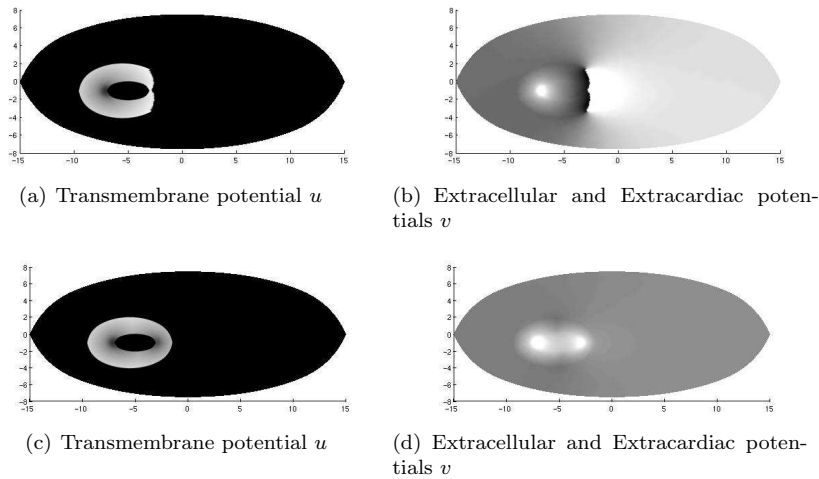
(a) Electrode 1   (b) Electrode 2   (c) Electrode 3   (d) Electrode 4

(e) Electrode 1   (f) Electrode 2   (g) Electrode 3   (h) Electrode 4

FIGURE 5.2. *ECGs for a 1 site stimulus (top) and a 2 sites stimulus (bottom) both at 100 bpm.*

(a) Transmembrane potential u (b) Extracellular and Extracardiac potentials v

(c) Transmembrane potential u (d) Extracellular and Extracardiac potentials v

FIGURE 5.3. *Potential Distributions at $t = 240$ ms for a stimulus at 100 bpm, on 1 site (top) and 2 sites (bottom).*

(a) Number of iterations for a residual of $1e-3$.

	Nothing	ILU0	ILU1
BiCGStab	43.8	7.1	6.9
GMRes	63.8	24.2	25.8

(b) CPU times for 100 linear systems.

residual	$1e-3$	$1e-5$	$1e-7$
BiCGStab	92	260	1012
GMRes	112	1253	

TABLE 5.1
Preconditioning

introduced above is used. The ionic model from Faber and Rudy is still used. The results are shown in figure 5.4. There are several very interesting facts. First, after a transitional period, a regular beat appears which has no T wave. It is also worth noticing that the right stimulus does only play a role on the first beat. After, it always
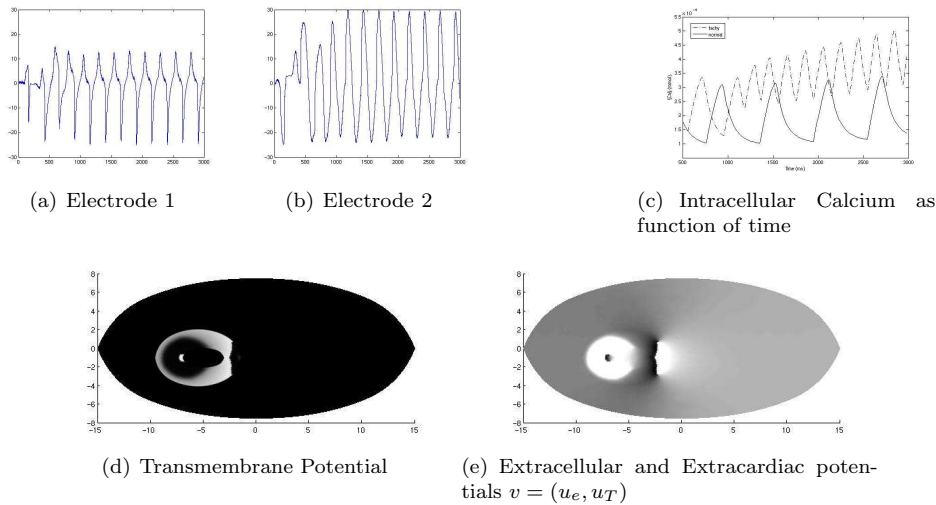
(a) Electrode 1   (b) Electrode 2   (c) Intracellular Calcium as function of time

(d) Transmembrane Potential   (e) Extracellular and Extracardiac potentials $v = (u_e, u_T)$

FIGURE 5.4. *ECGs and potential Distributions at $t = 240$ ms for a stimulus at 240 bpm: tachycardia*
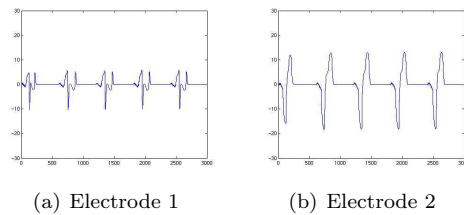

(a) Electrode 1   (b) Electrode 2

FIGURE 5.5. *Ischemia*

occurs in a zone where the *Na u*-dependent gates are closed and thus cannot have any effect (see the shape of *u* figure 5.4). At last the intracellular Calcium accumulates, whereas it resumes back to equilibrium for a regular beat, see figure 5.4(c).

Ischemia can also be simulated using Shaw and Rudy's improved Luo-Rudy II model ([SR97]). This disease is characterized by acidosis, anoxia and elevated concentration of extracellular potassium. The computed ECGs as shown in figure 5.5. There are modified as expected (modified amplitude as compared to a regular heartbeat).

6. A Bidomain Computation on a 3D experimental domain. 3D ECGs could not be computed yet, because adequate meshes are missing up to now. Indeed, a realistic simulation needs a very fine mesh of the 3D heart and the torso together with the data of the fibers directions in the heart. Hence, an anisotropic bidomain computation has been performed on a 3D mesh of data obtained by dissection of a canine heart at the university of Auckland, New Zeland (see [SCD$^+$01]) considered isolated ($T = \emptyset$ and there is no extracardiac potential function, $v = u_e$). The mesh consists in 8363 volumes and 3763 vertexes (12126 DDFV unknowns), together with fibers directions. Faber-Rudy's improvement of Luo-Rudy II model has been used for the computation of ionic currents. The parameters of the previous 2D computations

(a) $t = 50$ ms   (b) $t = 70$ ms   (c) $t = 120$ ms   (d) $t = 140$ ms
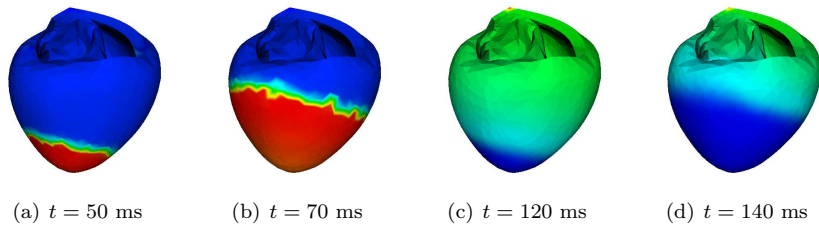
FIGURE 6.1. *Example of a 3D Computation*

are used, except $A_m = 100$. The mesh is too coarse for larger values of A_m to be used (in that case, a *propagation failure* phenomena would occur). The results are shown in figure 6.1, where the regions at rest are in blue while the activated regions are in red. Figure 6.1(a) and (b) shows the depolarization of the ventricles, figure 6.1(c) and (d) shows its repolarization.

REFERENCES

[ABH07]   B. Andreianov, F. Boyer, and F. Hubert. Discrete duality finite volume schemes for Leray-Lions-type elliptic problems on general 2d meshes. *Num. Meth. for PDEs*, 23(1):145–195, 2007. http://dx.doi.org/10.1002/num.20170.

[BCP09]   Y. Bourgault, Y. Coudière, and C. Pierre. Existence and uniqueness of the solution for the bidomain model used in cardiac electrophysiology. *Nonlinear Anal. Real World Appl.*, 10(1):458–482, 2009. DOI:doi:10.1016/j.nonrwa.2007.10.007.

[CFDE+05] P. Colli Franzone, P. Deuflhard, B. Erdmann, J. Lang, and L.F. Pavarino. Adaptivity in space and time for reaction-diffusion systems in electrocardiology. Technical report, Konrad-Zuze-Zentrum für Informationstechnik Berlin, 2005.

[CPT08]   Y. Coudière, C. Pierre, and R. Turpault. A ddfv scheme for anisotropic and heterogeneous elliptic equations, application to a bio-mathematics problem: Electrocardiogram simulation. In *Finite Volume For Complex Applications, Problems And Perspectives. 5th International Conference.* London (UK) Wiley, 2008.

[DO05]   K. Domelevo and P. Omnes. A finite volume method for the laplace equation on almost arbitrary two-dimensional grids. *M2AN*, 39(6):1203–1249, 2005.

[FR00]   G. Faber and Y. Rudy. Action Potential and Contractility Changes in [Na+]i Overloaded Cardiac Myocytes: A Simulation Study. *Biophysical Journal*, 78:2392–2404, 2000.

[KN94]   W. Krassowska and J.C. Neu. Effective boundary conditions for syncytial tissues. *IEEE*, 41(2):143–150, 1994.

[KS98]   J.P. Keener and J. Sneyd. *Mathematical Physiology.* Springer-Verlag, 1998.

[LBG+03]   G.T. Lines, M.L. Buist, A.J. Grottum, J. Sundnes, and A. Tveito. Mathematical models and numerical methods for the forward problem in cardiac electrophysiology. *Comput. Visual. Sci.*, (5):215–239, 2003.

[Pie05]   C. Pierre. *Modélisation et simulation de l'activité électrique du coeur dans le thorax, analyse numérique et méthodes de volumes.* PhD thesis, Université de Nantes, 2005.

[SCD+01]   M. Sermesant, Y. Coudière, H. Delingette, N. Ayache, and J.A. Désidéri. An electromechanical model of the heart for cardiac image analysis. In W. J. Niessen and M. A. Viergever, editors, *Medical Image Computed and Computer-Assisted Intervention*, number 2208 in LNCS, pages 224–231, 2001.

[SR97]   R.M. Shaw and Y. Rudy. Electrophysiologic Effects of Acute Myocardial Ischemia: a Theoretical Study of Altered Cell Excitability and Action Potential Duration. *Cardiovascular Research*, 35:256–272, 1997.

[ZLRR95]   J. Zeng, K.R. Laurita, D.S. Rosenbaum, and Y. Rudy. Two Components of the Delayed Rectifier K+ Current in Ventricular Myocytes of the Guinea Pig Type. *Circulation Research*, 77:140–152, 1995.